Supporting Information

Synergetic Effects of Electrochemical Oxidation of Spiro-OMeTAD and Li^+ Migration in Improving the Performance of n-i-p Type Perovskite Solar Cells

Changzeng Ding, Rong Huang, Christian Ahläng, Jian Lin, Lianping Zhang, Dongyu Zhang, Qun Luo, Fangsen Li, Ronald Österbacka, Chang-Qi Ma **

1. proposed oxidation mechanism reported in the literature:

Dye + hv --- Dye* --- Dye+ + $e^-(TiO_2)$ (1)

$e^-(TiO_2)$ + O_2 --- O_2^- (2)

Dye+ + Spiro-OMeTAD --- Spiro-OMeTAD$^+$ + Dye (3)

Scheme S1. proposed oxidation mechanism of Spiro-OMeTAD in solid state dye sensi tized solar cells.[1]

Spiro-OMeTAD + O_2 = Spiro-OMeTAD·O_2 (4)

Spiro-OMeTAD·O_2 + LiTFSI = Spiro-OMeTAD$^+$TFSI$^-$ + Li_xO_y (5)

Scheme S2. proposed oxidation mechanism of Spiro-OMeTAD by Snaith et al.[2]

Light Wavelength: 380-450nm

$$\text{Spiro-OMeTAD} + O_2 \xrightarrow{hv} \text{Spiro-OMeTAD}^{\cdot+} O_2^{\cdot-}$$

$$\text{Spiro-OMeTAD}^+O_2^{\cdot-} + Li^+TFSI^- \longrightarrow \text{Spiro-OMeTAD}^{\cdot+}TFSI^- + Li_xO_y$$

Light Wavelength: ＞450nm

$$\text{Perovskite} + O_2 \xrightarrow{hv} \text{Perovskite}^+ O_2^{\cdot-}$$

$$\text{Perovskite}^+ O_2^{\cdot-} + \text{Spiro-OMeTAD} \longrightarrow \text{Perovskite} + \text{Spiro-OMeTAD}^{\cdot+} O_2^{\cdot-}$$

$$\text{Spiro-OMeTAD}^{\cdot+}O_2^{\cdot-} + Li^+TFSI^- \longrightarrow \text{Spiro-OMeTAD}^+TFSI^- + Li_xO_y$$

Scheme S3. proposed oxidation mechanism of Spiro-OMeTAD by Meng et al.[3]

Figure S1. Statistical graph of changes in device performance and subsequent oxidation treatment time with fresh devices.(a) Voc, (b), Jsc, (c) FF, (d) PCE.

Figure S2 Comparison of the current density-voltage (J-V) curves of the same cell as shown in Figure 1b (a) and Figure 1c (b) with muliple scan.

Figure S3. The time-dependent curves of device performance parameters under different oxidation conditions (a) Voc (b) Jsc (c) FF (d) PCE

Figure S4. UV-Vis absorption spectra of (a). Glass/Spiro-OMeTAD (50% Li-TFSI:*t*-BP); (b). Glass/Spiro-OMeTAD (50% Li-TFSI:*t*-BP)/Ag;(c) Glass/SnO2/Spiro-OMeTAD (50% Li-TFSI:*t*-BP) films exposure in 30%RH air for different times. (d). Comparison of absorbance changes of the Spiro-OMeTAD films with or without SnO_2 layer.

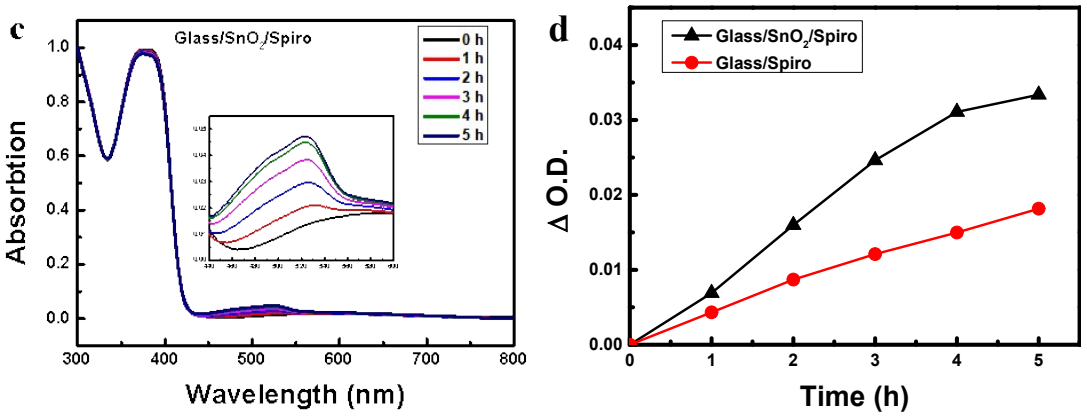

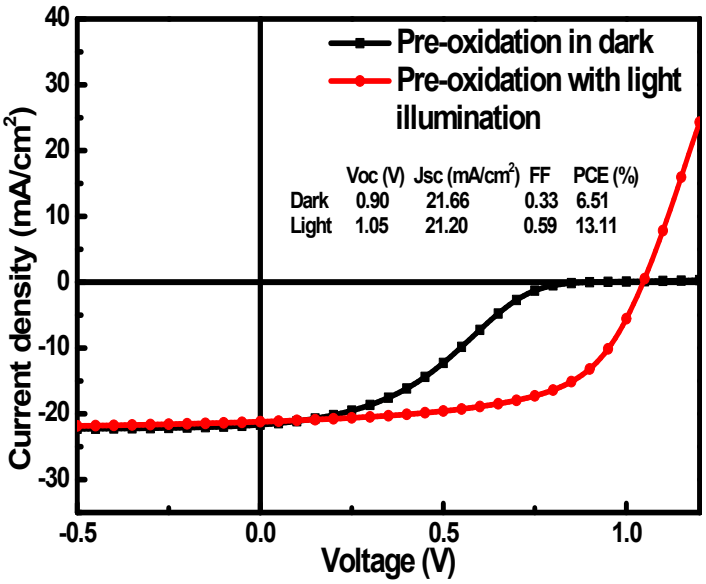

Figure S5. Current density-voltage (J-V) curves of Pre-oxidation cells in the dark and with light illumination.

Figure S6. Statistical graph of changes in device performance and subsequent oxidation treatment time after pre-oxidation .(a) Voc, (b), Jsc, (c) FF, (d) PCE.

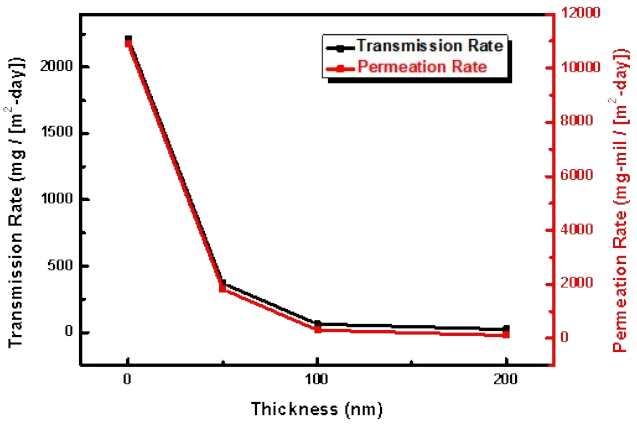

Figure S7. water vapor transmission rate (WVTR) of PET (125 μm)/Ag (x nm) film tested at 100%RH atmosphere

Figure S8 The variation of performance of devices with different thickness of Ag electrode

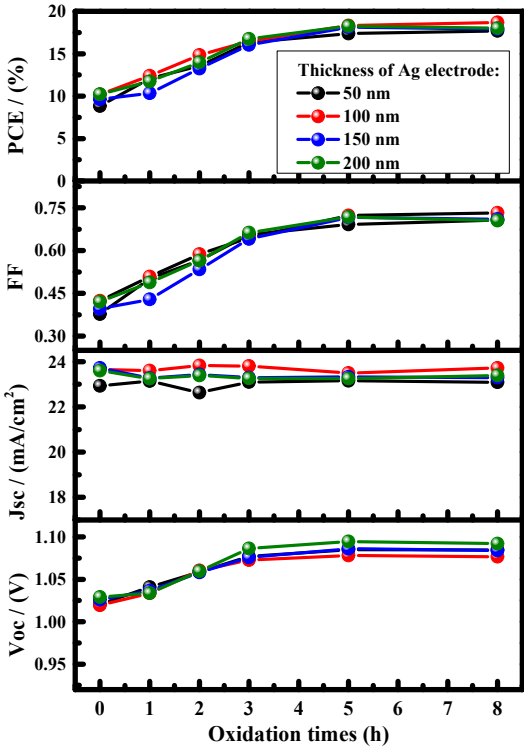

during oxidation process. Note that all the devices were pre-oxidized for 5 h in air with control RH of 30% in the dark.

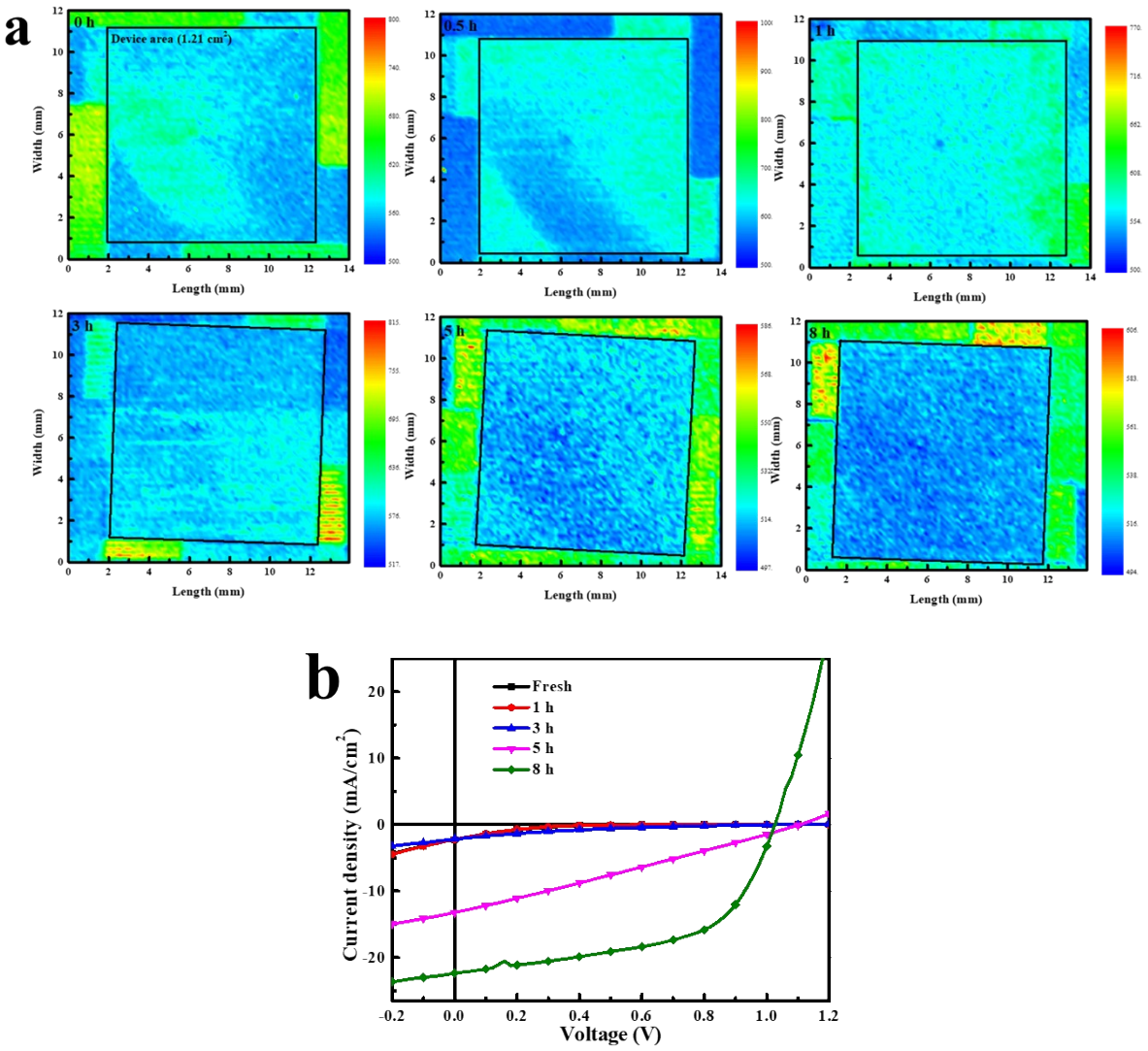

Figure S9. (a) PL-mapping of perovskite solar cells during the oxidation process in 30% RH air atmosphere, and the active area of solar cell is 1.21 cm^2. (b) J-V characteristics of the cell upon oxidation are also included.

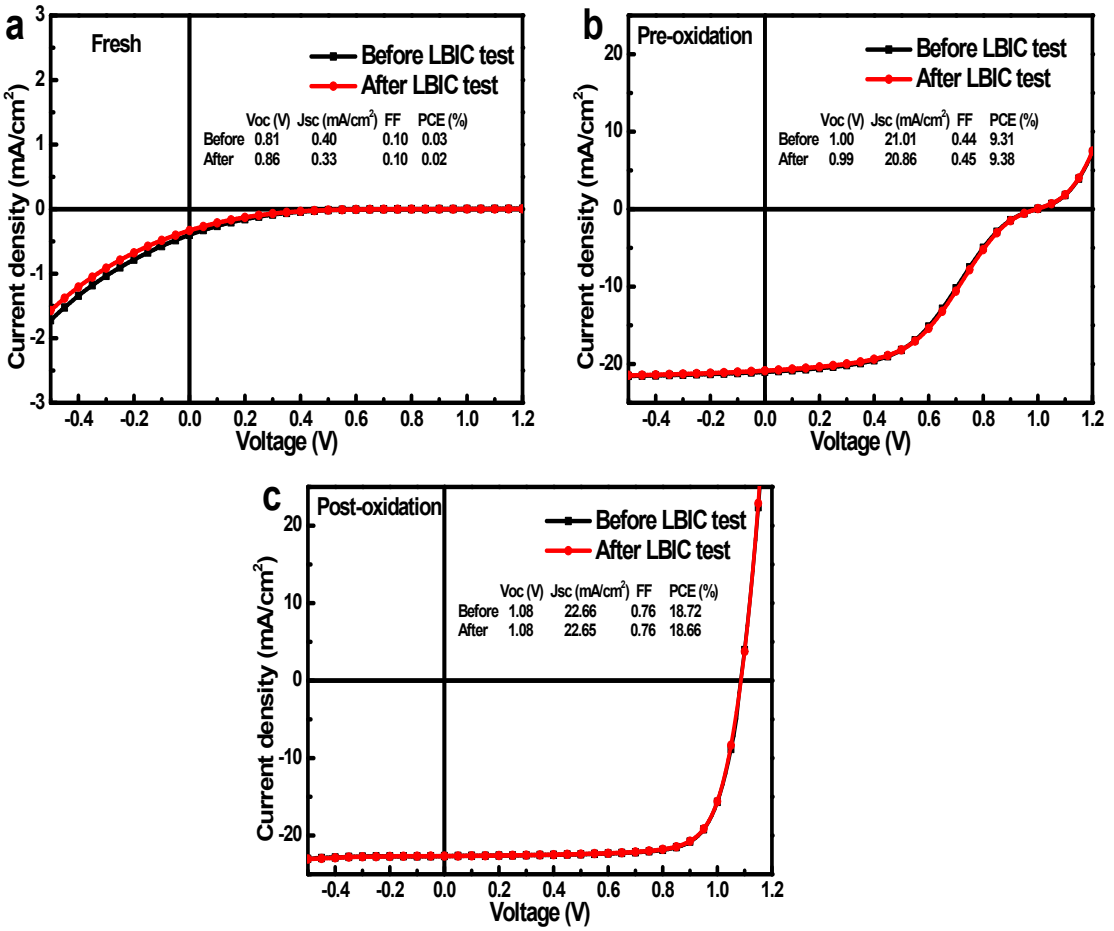

Figure S10 Current density-voltage (J-V) curves before and after LBIC test under different oxidation conditions a) Fresh, b) Pre-oxidation, c) Post-oxidation.

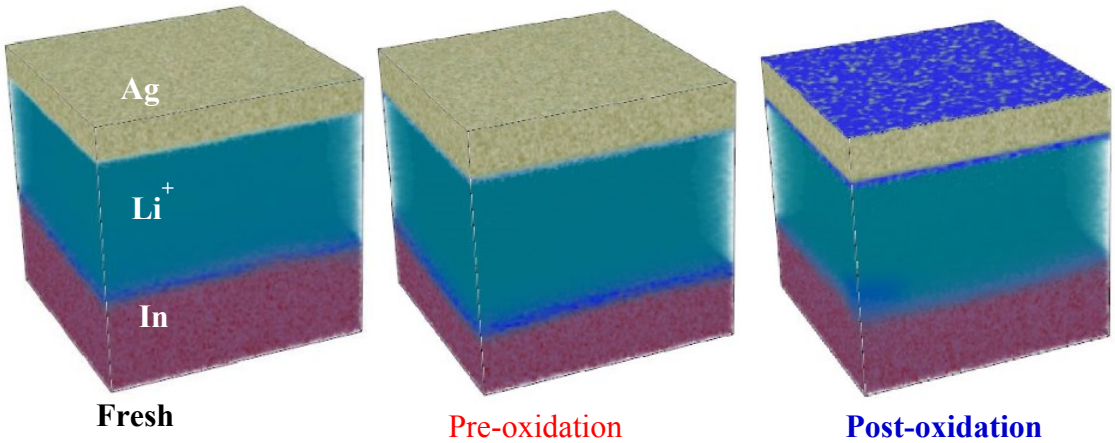

Figure S11. the distribution of Li^+ in ITO/Spiro/Ag films before and after oxidation in 3D configuration

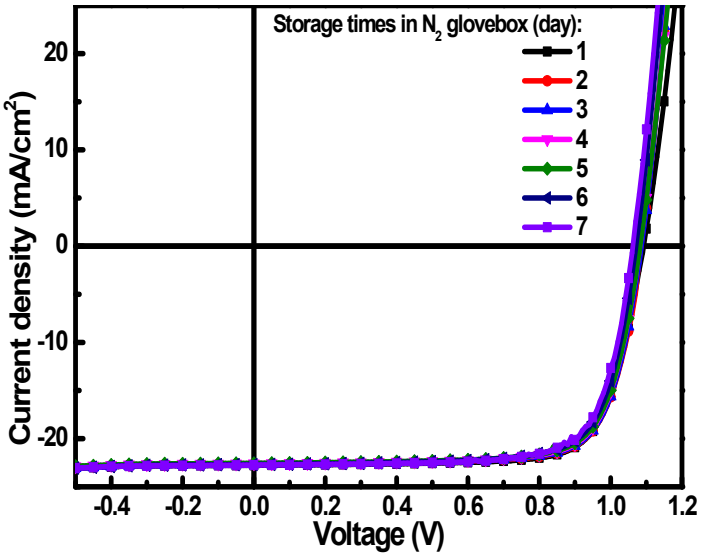

Figure S12. The evolution of J-V curves within a week for the optimized cell storage in dark in glove box.

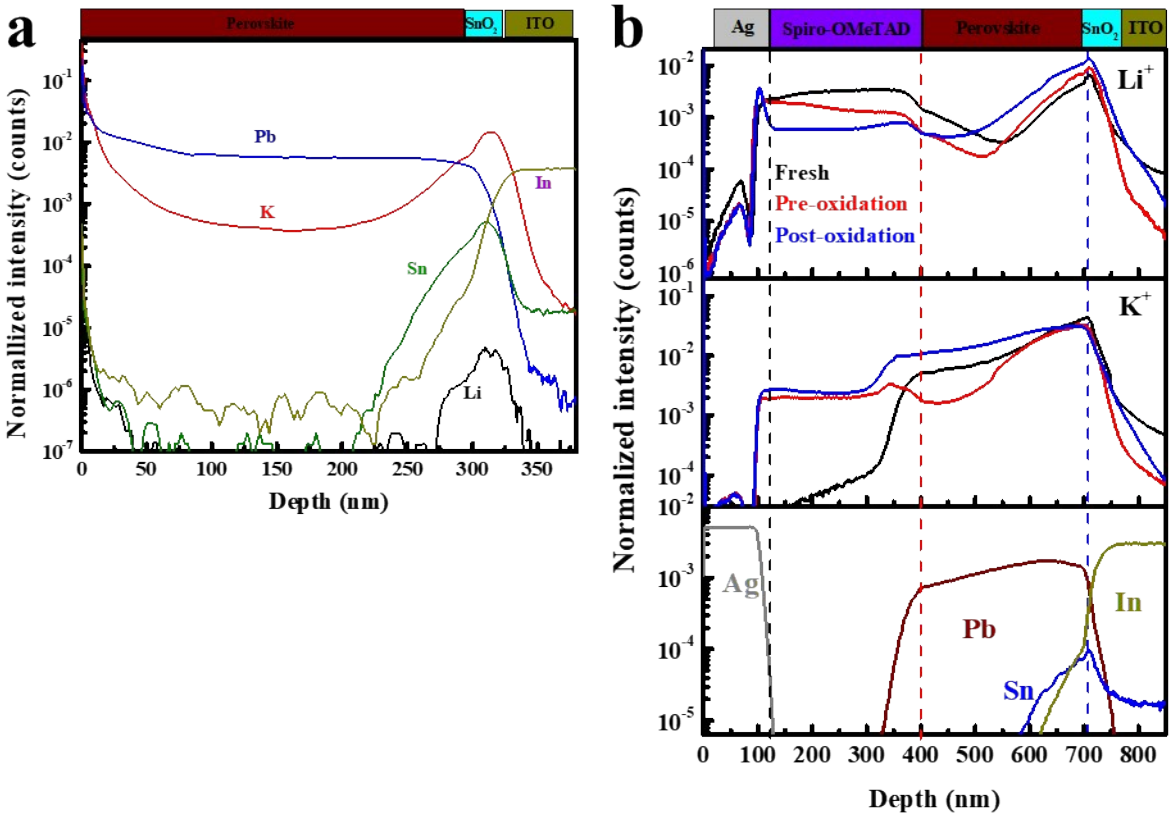

Figure S13. TOF-SIMS results of (a) Glass/ITO/SnO_2/PVSK and (b) diffusion of Li^+ and K^+ of the perovskite solar cell upon pre- and post-oxidation process.

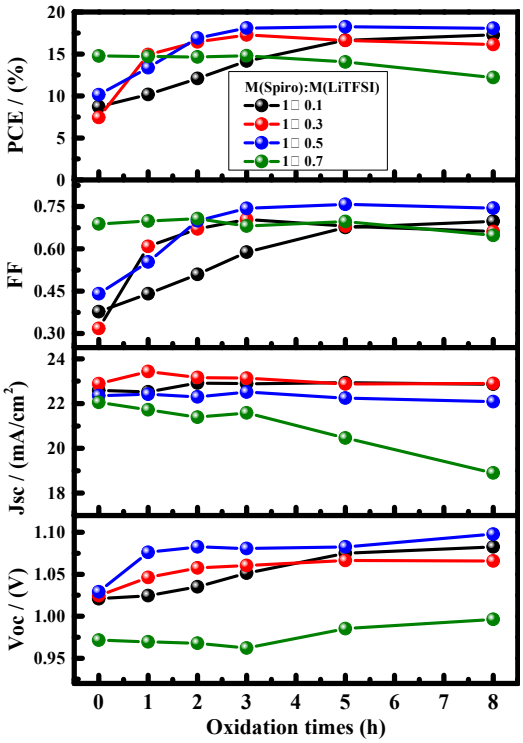

Figure S14 The variation of performance of devices doped with different concentrations of LiTFSI with oxidation time. Note that all the devices were pre-oxidized for 5 h in air with control RH of 30% in the dark.

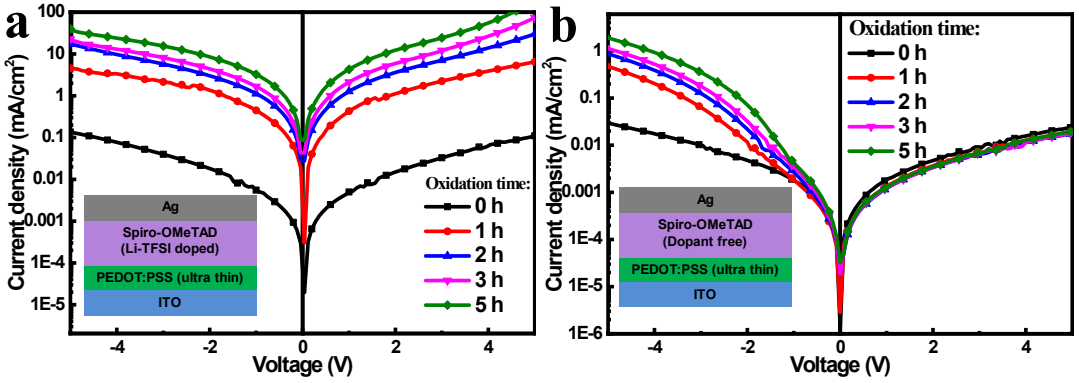

Figure S15. *J-V* curves of the dopant-free (a) and 50% LiTFSI-doped (b) Spiro-OMeTAD based hole only device upon different oxidation conditions.

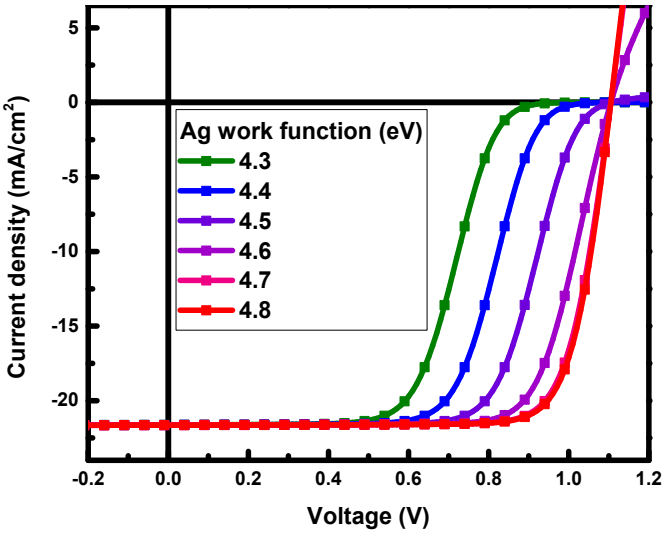

Figure S16. shows the effect of a change in the Ag work function, assuming that the doping concentration in the Spiro-OMeTAD layer is $3x10^{18}$ cm^{-3} and that the SnO_2 layer is ideal. Assuming that the Ag work function has a work function of 4.3 eV when it is fresh and goes down to 4.8 eV or lower upon oxidation, this could be the origin of the observed s-shapes.

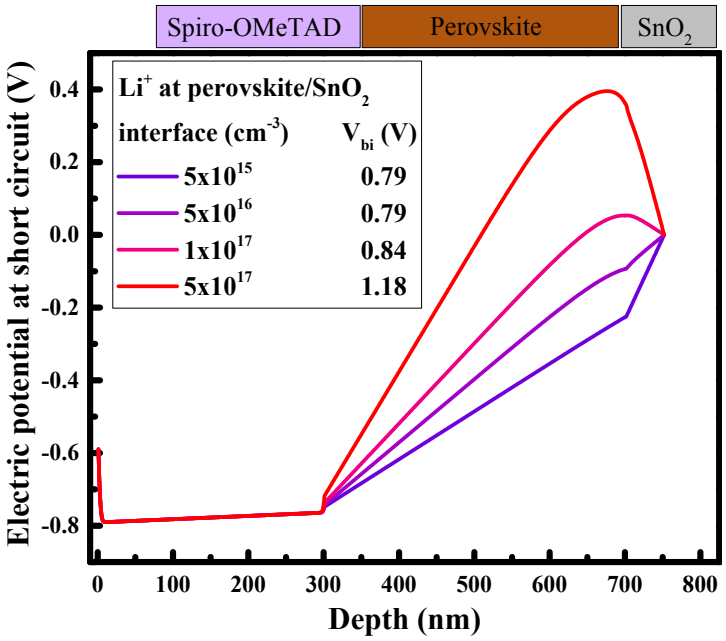

Figure S17 Electrical potential at short circuit for the simulation data show in Figure 4 (e). The built-in potential is estimated as the maximum potential difference for each curve.

Table S1. shows the parameters used in the drift-diffusion simulations. For the ideal SnO_2, we took the surface recombination velocity for holes to be 0.01 cm/s.

Parameter	Spiro-OMeTAD	Perovskite	SnO_2 (non-ideal)
Thickness (nm)	300	400	50
Electron transport level (eV)	2.0	3.5	3.6
Hole transport level (eV)	5.0	5.2	7.0
Effective density of state (cm^{-3})	10^{20}	5×10^{19}	10^{20}
Electron mobility (cm^2/Vs)	-	20	1
Hole mobility (cm^2/Vs)	5×10^{-5}	20	-
Relative dielectric constant	3	30	10
Electron trap-assisted recombination lifetime (ns)	10 (at perovskite interface)	100	1 (at perovskite interface)
Hole trap-assisted recombination lifetime (ns)	1 (at perovskite interface)	10	10 (at perovskite interface)
Radiative recombination coefficient (cm^3/s)	-	10^{-10}	-
Generation rate ($cm^{-3}\bullet s^{-1}$)	-	3.4×10^{21}	-
Injection barrier (eV)	0.3 (from Ag）	0.1 (from the ideal SnO_2)	0.5 （from ITO)

Table S2. The time-resolved photoluminescence (TRPL) fitting results.

	τ_1 (ns)	**τ_2 (ns)**
Fresh	22.62	53.99
Pre-oxidation	7.46	35.46
Post-oxidation	4.77	29.86

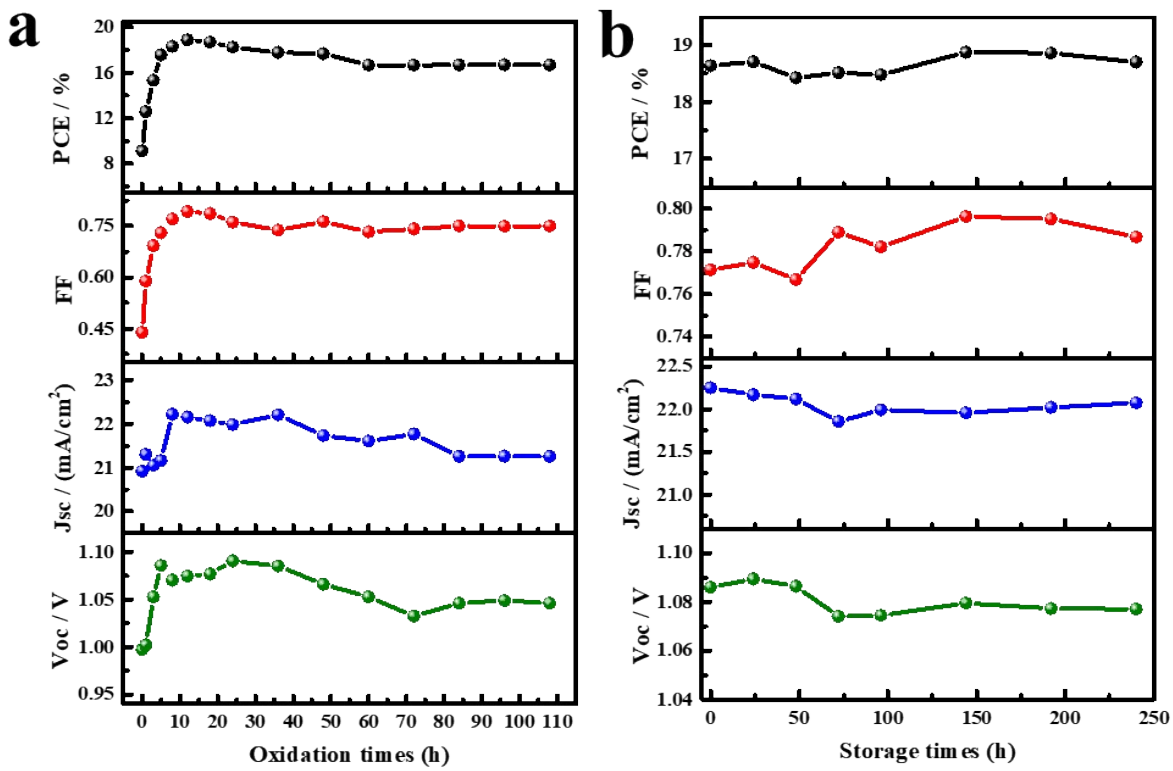

Figure S18 The variation of performance of the solar cells (a) with different oxidation times in 30% RH ambient air. (b) storage in N_2 glove box after post-oxidation for 8 h.

References:

1. U. B. Cappel, T. Daeneke and U. Bach, *Nano Lett.*, 2012, **12**, 4925-4931.
2. A. Abate, T. Leijtens, S. Pathak, J. l. Teuscher, R. Avolio, M. E. Errico, J. Kirkpatrik, J. M. Ball, P. Docampo, I. McPhersonc and H. J. Snaith, *Phys. Chem. Chem. Phys.*, 2013, **15**, 2572-2579.
3. S. Wang, W. Yuan and Y. S. Meng, *ACS Appl. Mater. Inter.*, 2015, **7**, 24791-24798.